JACC: CLINICAL ELECTROPHYSIOLOGY
VOL. 3, NO. 3, 2017

ISSN 2405-500X/$36.00
PUBLISHED BY ELSEVIER
http://dx.doi.org/10.1016/j.jacep.2016.12.016

High-Resolution Mapping of Ventricular Scar

Evaluation of a Novel Integrated Multielectrode Mapping and Ablation Catheter

Eran Leshem, MD,[a] Cory M. Tschabrunn, PhD,[a] Jihye Jang, MSc,[b] John Whitaker, MD,[b] Israel Zilberman, DVM,[c] Christopher Beeckler, BSc,[c] Assaf Govari, PhD,[c] Josef Kautzner, MD,[d] Petr Peichl, MD,[d] Reza Nezafat, PhD,[b] Elad Anter, MD[a]

ABSTRACT

OBJECTIVES This study sought to evaluate an investigational catheter that incorporates 3 microelectrodes embedded along the circumference of a standard 3.5-mm open-irrigated catheter.

BACKGROUND Mapping resolution is influenced by both electrode size and interelectrode spacing. Multielectrode mapping catheters enhance mapping resolution within scar compared with standard ablation catheters; however, this requires the use of 2 separate catheters for mapping and ablation.

METHODS Six swine with healed infarction and 2 healthy controls underwent mapping of the left ventricle using a THERMOCOOL SMARTTOUCH SF catheter with 3 additional microelectrodes (0.167 mm^2) along its circumference (Qdot, Biosense Webster, Diamond Bar, California). Mapping resolution in healthy and scarred tissue was compared between the standard electrodes and microelectrodes using electrogram characteristics, cardiac magnetic resonance, and histology.

RESULTS In healthy myocardium, bipolar voltage amplitude was similar between the standard electrodes and microelectrodes, with a fifth percentile of 1.19 and 1.30 mV, respectively. In healed infarction, the area of low bipolar voltage (defined as <1.5 mV) was smaller with microelectrodes (16.8 cm^2 vs. 25.3 cm^2; $p = 0.033$). Specifically, the microelectrodes detected zones of increased bipolar voltage amplitude, with normal electrogram characteristics occurring at the end of or after the QRS, consistent with channels of preserved subendocardium. Identification of surviving subendocardium by the microelectrodes was consistent with cardiac magnetic resonance and histology. The microelectrodes also improved distinction between near-field and far-field electrograms, with more precise identification of scar border zones.

CONCLUSIONS This novel catheter combines high-resolution mapping and radiofrequency ablation with an open-irrigated, tissue contact–sensing technology. It improves scar mapping resolution while limiting the need for and cost associated with the use of a separate mapping catheter. (J Am Coll Cardiol EP 2017;3:220–31)

From the [a]Harvard-Thorndike Electrophysiology Institute Cardiovascular Division, Department of Medicine, Beth Israel Deaconess Medical Center, Harvard Medical School, Boston, Massachusetts; [b]Cardiovascular Division, Department of Medicine, Beth Israel Deaconess Medical Center, Harvard Medical School, Boston, Massachusetts; [c]Biosense Webster, Research and Development, Diamond Bar, California; and [d]Department of Cardiology, Institute for Clinical and Experimental Medicine (IKEM), Vídeňská, Prague, Czech Republic. This study was supported in part by an investigator-initiated grant from Biosense Webster (a Johnson & Johnson company); and a National Institutes of Health grant 1R21HL127650-01. Dr. Leshem is the recipient of a National Institutes of Health training grant (5T32HL007374-37). Dr. Tschabrunn has received research grants from Biosense Webster and has served as a consultant to Boston Scientific. Dr. Zilberman, Mr. Beeckler, and Dr. Govari are Biosense Webster (a Johnson & Johnson company) employees. Dr. Kautzner has received speaker honoraria from Biosense Webster, Medtronic, LivaNova, and St. Jude Medical, has served as a consultant for Biosense Webster, and has served on advisory boards for Biosense Webster, Boston Scientific, Medtronic, LivaNova, and St. Jude Medical. Dr. Anter has received research grants from Biosense Webster and Boston Scientific. All other authors have reported that they have no relationships relevant to the contents of this paper to disclose.
All authors attest they are in compliance with human studies committees and animal welfare regulations of the authors' institutions and Food and Drug Administration guidelines, including patient consent where appropriate. For more information, visit the *JACC: Clinical Electrophysiology* author instructions page.

Manuscript received September 28, 2016; revised manuscript received November 17, 2016, accepted December 1, 2016.

Reentry is a common mechanism of scar-related atrial and ventricular arrhythmias. It usually develops in the presence of inhomogeneous scar tissue with various degrees of surviving myocardial bundles, providing the necessary conduction slowing for reentry (1).

Mapping scar-related reentrant arrhythmias requires identification of low-amplitude diastolic electrograms during tachycardia (activation mapping) or the identification of channels of surviving myocardial bundles during sinus or paced rhythm (substrate mapping). The resolution of electrical mapping is determined by multiple parameters, including the mapping rhythm, vector of propagation, electrode size, interelectrode spacing, and filtering. Standard linear ablation catheters have a 3.5-mm distal electrode separated by 1 mm from a proximal 1-mm electrode, resulting in a center-to-center interelectrode spacing of 3.25 mm. As such, each bipolar electrogram represents an underlying tissue diameter ranging from 3.5 to 5.5 mm, depending on the angle of incidence (from perpendicular to parallel to the tissue, respectively) (2,3). This sampling resolution is often insufficient for identifying and selectively pacing channels of surviving myocardial bundles embedded in surrounding scar tissue. The use of multielectrode mapping catheters with smaller electrode and interelectrode spacing can increase the resolution of mapping, enhancing identification of surviving channels and macro-re-entrant circuits (2,4–7). However, the use of 2 separate catheters is often associated with the need for additional vascular access (including transseptal puncture), increased mapping time to navigate the ablation catheter to the identified site of interest, and procedural cost.

In this study, we report a new catheter technology that integrates a standard open-irrigated ablation catheter with tissue-sensing contact force technology and 3 microelectrodes embedded along the circumference of the distal electrode. This setting allows for high-resolution mapping along with ablation capabilities in a single catheter. We compared the mapping resolution of the standard electrodes and the microelectrodes in healthy and scarred left ventricle (LV).

METHODS

EXPERIMENTAL STUDY DESIGN. This prospective study included a total of 8 swine, 2 healthy controls and 6 with chronic anterior wall infarction. We have recently described our swine model of chronic left anterior descending coronary artery (LAD) occlusion that closely approximates human subendocardial infarction and reentrant ventricular tachycardia (VT) (8). In brief, Yorkshire swine (male; weight: 30 to 35 kg) underwent selective balloon occlusion of the LAD for 180 min. After a survival period of 4 to 6 weeks, animals underwent in vivo cardiac magnetic resonance (CMR) imaging, electroanatomic mapping (EAM) of the LV, subsequent ex vivo CMR, and histological analysis. The institutional animal care and use committee approved this research protocol.

ABBREVIATIONS AND ACRONYMS

CMR = cardiac magnetic resonance

EAM = electroanatomic mapping

LAD = left anterior descending coronary artery

LGE = late gadolinium enhancement

LV = left ventricle

VT = ventricular tachycardia

INVESTIGATIONAL CATHETER DESIGN. This investigational catheter (Qdot, THERMOCOOL SMARTTOUCH SF-5D Catheter, Biosense Webster, Diamond Bar, California) incorporates 3 microelectrodes, each with a surface area of 0.167 mm^2 embedded at the distal circumference of a standard 3.5-mm open-irrigated catheter (**Figure 1**). The standard mapping electrodes consist of a distal 3.5-mm electrode (M_1) separated by 1 mm from the proximal 1-mm electrode (M_2). The bipolar electrogram is formed by subtraction of their unipolar electrograms (M_1-M_2). Simultaneously, each microelectrode records a unipolar electrogram, generating 3 bipolar configurations (Mic_1-Mic_2, Mic_2-Mic_3, and Mic_3-Mic_1). Thus, each acquisition point consists of 4 bipolar electrograms: one from the standard mapping electrodes (M_1-M_2) and 3 from the microelectrodes. In addition to recording from smaller tissue size, the microelectrodes record data at multiple angles relative to the vector of propagation (from parallel to perpendicular), which increases the ability to detect surviving myocardial bundles. Radiofrequency energy can be delivered from the distal 3.5-mm electrode, whereas pacing can be performed from all electrodes in a unipolar or bipolar configuration.

MAPPING PROTOCOL. EAM was performed under general anesthesia with the CARTO 3 mapping system (Biosense Webster). A quadripolar catheter was positioned at the right ventricular apex to serve as an intracardiac activation reference. Mapping of the LV was performed during right ventricular apical pacing. The investigational mapping catheter was advanced into the LV via a retrograde transaortic approach. Data points were acquired by slowly navigating the catheter in the LV. Each data point was acquired with the catheter at a stable position, with a contact force range between 5 and 40 g and beat-to-beat electrogram stability of ≥2 sequential beats. The map was considered complete when the point density allowed interpolation to be limited to ≤15 mm in normal tissue and ≤5 mm in regions of low bipolar voltage amplitude (defined as ≤1.5 mV using the standard

FIGURE 1 Structure of the Investigational Catheter

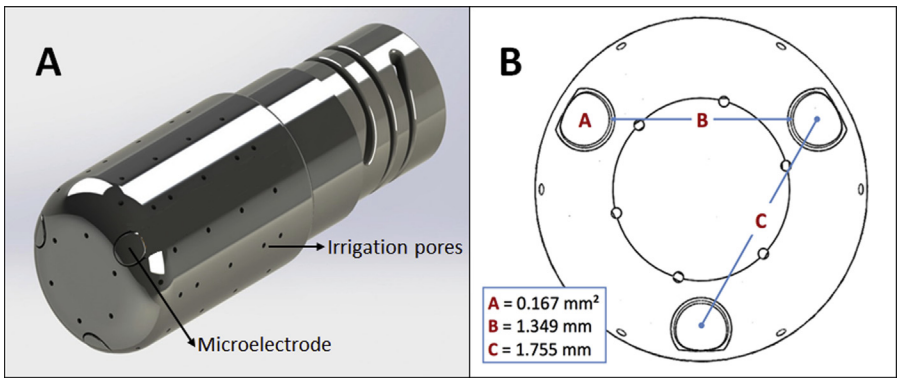

(A) Qdot Catheter (THERMOCOOL SMARTTOUCH SF-5D Catheter, Biosense Webster) incorporating 3 microelectrodes at the tip of the standard 3.5-mm electrode tip. **(B)** Schematic of distal surface of the catheter, highlighting the 3 microelectrodes, each with a surface area of 0.167 mm^2 **("A" in red)**. **B and C** are the distances between neighboring microelectrodes (minimal distance and center to center).

M_1-M_2 electrodes). The microelectrode map was created by using the maximal amplitude acquired at that point by 1 of 3 microelectrode signals (the highest voltage among Mic1-Mic2, Mic2-Mic3, and Mic3-Mic1 for each point). Bipolar electrograms were filtered between 8 and 500 Hz and unipolar electrograms between 0.5 and 240 Hz. Unipolar electrograms were constructed between each of the mapping electrodes and Wilson's central terminal.

PACING PROTOCOL. Pacing from low-voltage areas can result in high-output capture or noncapture, which often limits pacing and entrainment techniques. Because smaller electrodes have higher current density, we hypothesized that the smaller microelectrodes might capture the tissue at a lower pacing threshold (2,4). We compared the pacing threshold between the standard electrodes and microelectrodes in the low-voltage area. In 4 infarcted swine, the catheter was positioned at ≥10 different low bipolar voltage sites per swine. At each site, pacing output was determined for the standard M_1-M_2 electrodes and for the microelectrodes at fixed pacing output duration of 2 ms. Failure to capture was defined as lack of tissue capture with 10 mA at 2 ms. Stimulation to QRS interval was measured at each site with tissue capture for both the standard electrodes and microelectrodes.

DEFINITIONS AND ELECTROGRAM ANALYSIS. The normal range of bipolar voltage amplitude and bipolar electrogram duration for the microelectrodes was calculated in 2 healthy ventricles. The lower bipolar voltage cutoff was defined as the fifth percentile of the bipolar voltage range for both the standard electrodes and microelectrodes. Electrogram duration was measured from the earliest initial deflection from the isoelectric line to the onset of the decay artifact produced by the amplified filtered signal of the bipolar electrogram as previously reported (9,10).

Abnormal bipolar electrograms were defined as follows: *fractionated electrograms* had ≥5 intrinsic deflections; *late potentials* were defined as electrograms with activation spanning ≥20 ms after the end of the surface QRS complex; *isolated late potentials* were defined as electrograms with an additional electrogram component after the end of the surface QRS complex that was separated by an isoelectric interval from the initial electrogram by ≥20 ms.

All electrograms were analyzed offline with electronic calipers at uniform lead gain of 1 mV and paper sweep speed of 200 mm/s.

CMR IMAGING. In vivo and ex vivo CMR imaging was performed with a 1.5-T magnetic resonance imaging scanner (Phillips Achieva, Best, the Netherlands). Three-dimensional late gadolinium enhancement (LGE) images with isotropic spatial resolution of 1 mm^3 were acquired 15 to 25 min after infusion of 0.2 mmol/kg gadobenate dimeglumine (MultiHance, Bracco, Rome, Italy). A respiratory navigator placed on the dome of the right hemidiaphragm with an adaptive acquisition window to achieve a fixed navigator efficiency of 60% (11) was used for prospective real-time correction. Three-dimensional random undersampling for the accelerated

acquisitions (12,13) was used for image reconstruction. Endocardial and epicardial contours were manually delineated in all slices, and LGE volume was defined using a full width at half maximum technique (14). Endocardial mesh was generated using Poisson surface reconstruction from manually drawn endocardial contours. LGE volume of the endocardial area (0% to 33% from endocardium to epicardium) was then projected onto the endocardial mesh. Surface area of the endocardium/scar was calculated based on the area of the triangular meshes of endocardium/scar. Mesh processing was performed with MeshLab (15).

HISTOPATHOLOGICAL ANALYSIS. After mapping procedures, the hearts were harvested and placed in a 10% buffered formalin solution for >1 week for tissue fixation, then were serially sectioned parallel to the atrioventricular groove into 1-cm thick slices starting from the apex. Tissue samples were paraffin embedded by use of large tissue histology cassettes. Tissue was sectioned at intervals of 500 μm with a 5-μm thickness, and slides were stained with Masson's trichrome for collagen detection and digitized. Regions of low bipolar voltage were examined for characterization of myocardial fibrosis and surviving tissue. Investigation of the approximate line of interest throughout the different modalities (EAM, histology, and CMR) was performed by measuring in CARTO 3 the distance from the apex and locating the corresponding histological slide and CMR plane at the exact distance.

STATISTICAL ANALYSIS. Descriptive statistics are reported as mean ± SD, median (range) for continuous variables and as absolute frequencies and percentages for categorical variables. Comparison between surface area of bipolar low voltage and pacing capture was calculated with the paired Student *t* test. Investigation of electrogram characteristics was performed with a hierarchical mixed-effect linear regression, modeling between-pig variability as a random effect. Bivariate correlation was performed with the Pearson r correlation coefficient. A p value < 0.05 was considered statistically significant. Statistical analyses were performed with SPSS software version 20 (SSPS, Chicago, Illinois).

RESULTS

MAPPING DATA AND ELECTROGRAM ANALYSIS. We analyzed 7,120 electrograms in 8 swine (890 ± 482; median 746; range 424 to 1,809). A total of 1,732 of these electrograms were excluded from the analysis because of inadequate beat selection criteria, which included nonpaced beats, fused beats, inadequate tissue contact force, and beat-to-beat electrogram inconsistency.

FIGURE 2 Electrogram Recordings With Standard and Microelectrodes in Healthy Ventricle

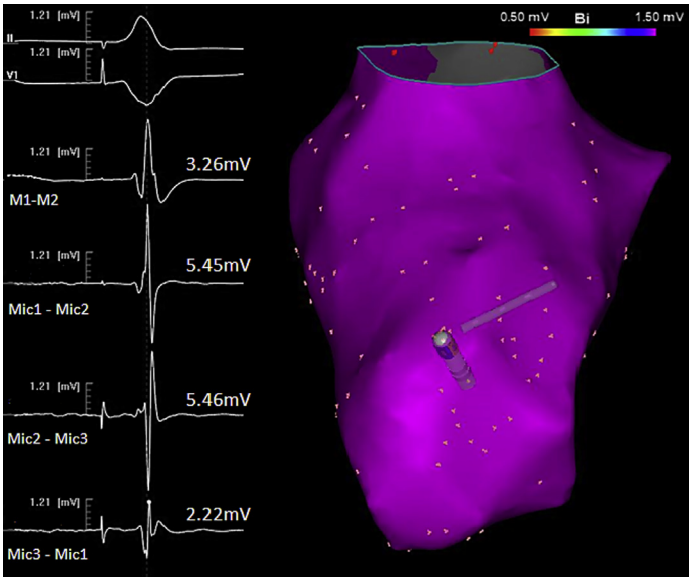

Electroanatomic map of healthy left ventricle in an anterior-posterior projection at a bipolar voltage range of 0.5 to 1.5 mV. Bipolar electrograms were recorded during right ventricular pacing. M1-M2 represents recording from the standard distal bipolar pair electrodes; Mic1-Mic2, Mic2-Mic3, and Mic3-Mic1 represent bipolar recording from the microelectrodes. Mean bipolar voltage amplitude was higher with microelectrodes; however, the fifth percentile cutoff values were similar between the standard electrodes and the microelectrodes. Electrograms recorded with microelectrodes had a shorter duration.

ELECTROGRAM CHARACTERISTICS IN THE HEALTHY VENTRICLE. Bipolar amplitude and duration. In the healthy LV, the bipolar electrogram amplitude measured with the microelectrodes was higher than that measured with the standard electrodes (4.5 ± 2.5 mV [median 3.9 mV] vs. 3.8 ± 2.3 mV [median 3.3 mV]; p < 0.001). The fifth percentile of the bipolar voltage distribution was similar between the microelectrodes and standard electrodes (1.30 mV vs. 1.19 mV, respectively). As such, we used the conventional definition of normal bipolar voltage amplitude ≥1.5 mV. The bipolar electrogram duration of the microelectrodes was shorter than that of standard electrodes (75 ± 10 ms [range 47 to 110 ms] vs. 84 ± 12 ms [range 52 to 122 ms]; p < 0.001). Figure 2 shows an example of electrograms recorded with standard electrodes and microelectrodes in healthy ventricle.

Unipolar amplitude. The unipolar electrogram amplitude measured with the microelectrodes was

lower than that measured with the standard electrodes (5.7 ± 2.3 mV [median 5.2 mV; range 2.1 to 15.4 mV] vs. 8.2 ± 2.9 mV [median 7.8 mV; range 2.9 to 22.4 mV]; $p < 0.001$). The fifth percentile of the unipolar voltage distribution was also lower with microelectrodes (2.9 mV vs. 4.1 mV).

Although both electrode types showed a positive correlation between the bipolar and unipolar voltage amplitude ($r = 0.50$ and $r = 0.51$, respectively) (Online Figure 1), the magnitude of increase in unipolar voltage amplitude compared with the corresponding increase in the bipolar voltage amplitude was lower with the microelectrodes. For every 1.0-mV increase in bipolar voltage amplitude recorded with standard electrodes, the corresponding unipolar amplitude increased by 0.65 mV, whereas for a similar 1.0-mV increase in bipolar voltage amplitude recorded with microelectrodes, the corresponding unipolar amplitude increased only by 0.48 mV. This could be related to the smaller field of view ("antenna") of the microelectrodes.

ELECTROGRAM CHARACTERISTICS IN THE POST-INFARCT VENTRICLE. In 6 swine with healed infarction, a total of 4,756 electrograms were analyzed. Of these, 3,424 (72%) were recorded within the area of low bipolar voltage (<1.5 mV) as defined by the standard electrodes. Within the low-voltage area, 1,605 of 3,424 electrograms (47%) were recorded in the very low-voltage zone (conventionally defined as ≤0.5 mV using the standard electrodes).

Electrogram amplitude. Bipolar voltage distribution within the low-voltage area was higher with the microelectrodes (1.0 ± 0.93 mV [median 0.67 mV] vs. 0.59 ± 0.34 mV [median 0.52 mV]; $p < 0.001$). In particular, within the area of very low voltage, the microelectrodes recorded significantly higher bipolar voltage amplitude (0.71 ± 0.58 mV vs. 0.30 ± 0.11 mV; $p < 0.001$). A comparison in bipolar voltage amplitude distribution in the low- and very low-voltage zone between the electrodes is shown in Online Figure 2.

The area of low bipolar voltage (<1.5 mV) was 33.6% smaller when assessed by microelectrodes than by standard electrodes (16.8 ± 3.3 cm^2 [range 13.1 to 22.6 cm^2] vs. 25.3 ± 7.4 cm^2 [range 15.9 to 35.1 cm^2]; $p = 0.033$). Area measurement using the 5% thresholds found for each electrode type in the normal swine (1.3 and 1.19 mV for the microelectrodes and standard electrodes, respectively) revealed slightly smaller low bipolar area for both the microelectrodes and standard electrodes (15.9 ± 2.7 cm^2 [range 12.0 to 20.1 cm^2] vs. 23.9 ± 7.6 cm^2 [range 15.9 to 34.4 cm^2]; $p = 0.049$). Particularly, the very low-voltage area (<0.5 mV) was 54.7% smaller when mapped with microelectrodes (3.8 ± 1.9 cm^2 [range 1.9 to 7.1 cm^2] vs. 8.3 ± 2.9 cm^2 [range 4.3 to 12.8 cm^2]; $p = 0.007$) comprising 2.4% versus 5.5% of the LV, respectively. Figure 3 shows an example of a bipolar voltage map comparing standard electrodes and microelectrodes.

Electrogram characteristics. Within the area of low voltage, electrograms recorded with microelectrodes had a shorter duration (82 ± 16 ms [range 31 to 139 ms] vs. 92 ± 15 ms [range 44 to 139 ms] respectively; $p < 0.001$). Electrograms recorded with microelectrodes within the area of low and very low voltage demonstrated a higher prevalence of healthy electrograms (triphasic with amplitude ≥1.5 mV), fractionated electrograms, and electrograms with late potentials. Healthy electrograms were recorded in 3.7% (89 of 2,559). Fractionated electrograms were recorded in 76% (1,944 of 2,559) compared with 52% (450 of 865) using standard electrodes. Late potentials were recorded in 42% (1,086 of 2,559) compared with 31% (267 of 865) using standard electrodes, and isolated late potentials were recorded in 2.5% (65 of 2,559) compared with 0.6% (5 of 865) using standard electrodes (Table 1, Figure 4).

Unipolar electrograms. The unipolar electrogram amplitude measured with microelectrodes was lower than that measured with standard electrodes (1.9 ± 1.2 mV [median 2.7 mV; range 0.2 to 22 mV] vs. 3.3 ± 1.3 mV [median 3.7 mV; range 0.2 to 27.8 mV]; $p < 0.001$). The fifth percentile of the unipolar voltage distribution was also lower when measured with microelectrodes (0.8 mV vs. 1.4 mV).

In the zone of low bipolar voltage amplitude, a positive correlation between the bipolar and unipolar was also observed ($r = 0.5$ and 0.34, respectively) (Online Figure 3). The magnitude of increase in unipolar voltage amplitude compared with the corresponding increase in the bipolar voltage amplitude was lower with the microelectrodes. For every 1.0-mV increase in bipolar voltage amplitude recorded with standard electrodes, the corresponding unipolar amplitude increased by 1.92 mV, whereas for a similar 1.0-mV increase in bipolar voltage amplitude recorded with microelectrodes, the corresponding unipolar amplitude increased only by 0.42 mV.

DEFINITION OF THE INFARCT BORDER. We compared the precision of the standard electrodes and microelectrodes for identifying the border between scar and healthy tissue (i.e., infarct border zone), because smaller electrodes record from smaller tissue size and are subjected to less averaging, and thus, they may be better suited to differentiate near-field from far-field electrograms. Mapping with microelectrodes demonstrated improved distinction

FIGURE 3 Differences in Mapping Scar With Standard vs. Microelectrodes

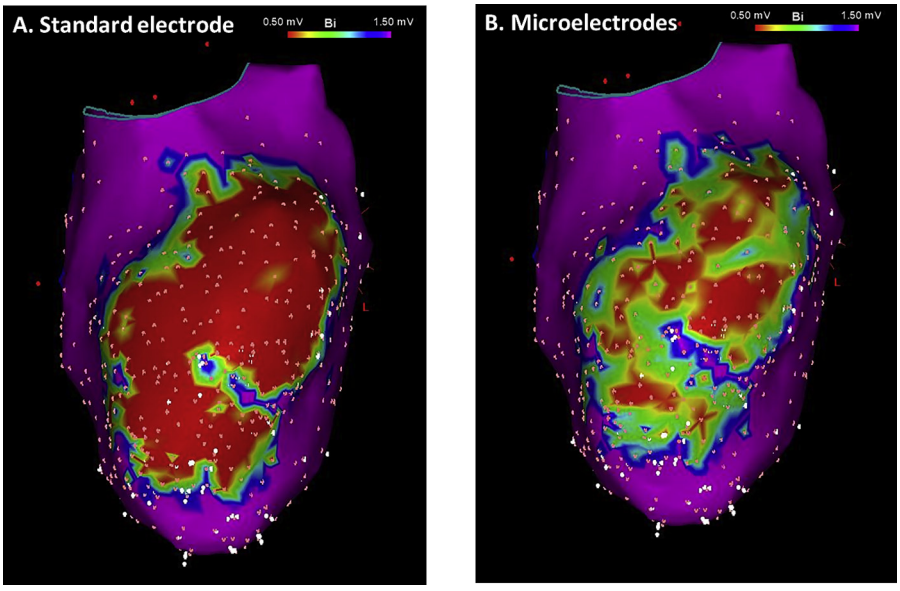

Mapping with standard electrodes shows a relatively homogenous area of very low-voltage "dense scar" (<0.5 mV). In contrast, mapping with microelectrodes shows an overall increased bipolar voltage amplitude with a significantly smaller zone of very dense scar. In addition, channels of increased voltage are recognized within the overall low-voltage area.

between scar and healthy tissue (Figure 5), allowing better differentiation between near-field and far-field signals at the scar border zone.

COMPARISON TO CMR. An extensive area of LGE at the anterior septum was observed in swine with healed LAD infarction. LGE distribution was complex, with areas of transmural or near transmural distribution along with areas of partial thickness involvement with sparring of the subendocardium. The overall LGE content was 11.5 ± 3% of the entire LV myocardial volume. The endocardial portion of the LGE comprised 34 ± 3% of the total scar volume. The mean LGE area projected on the endocardial surface was 21.8 ± 5.1 cm^2, and the scar percentage of the LV endocardial surface was 18.9 ± 4.5% (Figure 6). The endocardial LGE surface area corresponded to the EAM zone of bipolar voltage amplitude <1.5 mV as mapped with both the standard electrodes and the microelectrodes. However, channels of preserved subendocardium as identified by microelectrodes but not by standard electrodes corresponded to channels of preserved subendocardium on CMR (Figure 6).

COMPARISON TO HISTOLOGY. Histological analysis revealed complex scar architecture with areas of transmural scar, along with areas of partial thickness involvement limited to the mid-myocardium and subepicardium, with subendocardial preservation. The overall architecture and distribution of scar were consistent with the LGE data. Analysis of the subendocardial scar distribution showed heterogeneous collagen disposition with areas of preserved myocardial bundles within the scar. Although direct correlation between the histological specimen and the

TABLE 1 Electrogram Measurement Results in Low-Voltage Area (Bipolar Amplitude <1.5 mV) and Very Low-Voltage Area (Bipolar Amplitude <0.5 mV), as Defined by Standard Electrodes

	Standard Electrodes	Microelectrodes	p Value
Low bipolar voltage area			
Unipolar voltage (mV)	3.27 ± 1.29	1.92 ± 1.15	<0.001
Bipolar voltage (mV)	0.59 ± 0.34	1.0 ± 0.93	<0.001
Bipolar duration (ms)	92 ± 15	82 ± 16	<0.001
Bipolar fractionation ≥5	450 (52)	1,944 (76)	<0.001
Late potentials	267 (31)	1,086 (42)	<0.001
Very low bipolar voltage area			
Unipolar voltage (mV)	2.73 ± 1.01	1.66 ± 1.09	<0.001
Bipolar voltage (mV)	0.30 ± 0.11	0.71 ± 0.58	<0.001
Bipolar duration (ms)	97 ± 14	85 ± 15	<0.001
Bipolar fractionation ≥5	221 (55)	915 (76)	<0.001
Late potentials	168 (42)	662 (55)	<0.001

Values are mean ± SD or n (%).

FIGURE 4 Comparison of Electrogram Characteristics Within the Infarct Zone at 3 Different Locations

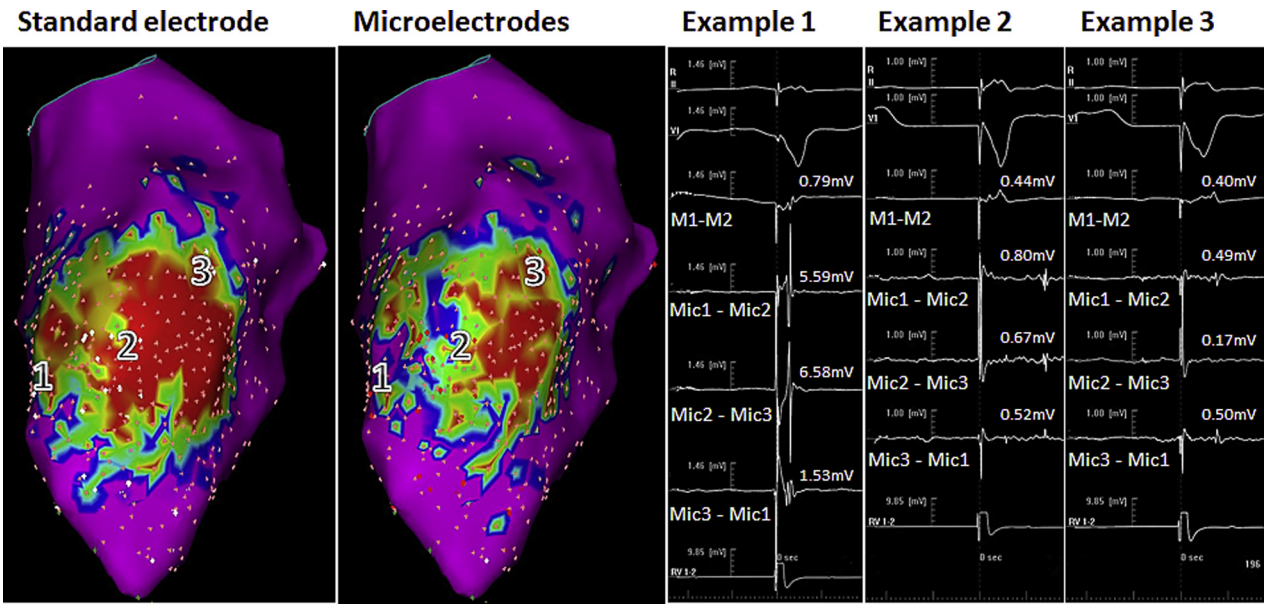

In location 1 at the septal border of the infarct, the standard M1-M2 electrogram shows a low-amplitude electrogram, whereas the microelectrodes (Mic1-Mic2, Mic2-Mic3, and Mic3-Mic1) show a narrow high-amplitude electrogram, improving delineation of the infarct border zone. In location 2, the microelectrodes record a distinct near-field late potential that is not shown with standard electrodes recorded simultaneously and gained similarly. Location 3, recorded at the lateral border of the infarct, shows low-amplitude electrogram that is similar for the standard electrodes and microelectrodes.

FIGURE 5 Electrogram Discrepancies at Border Zone Between Standard Electrodes and Microelectrodes

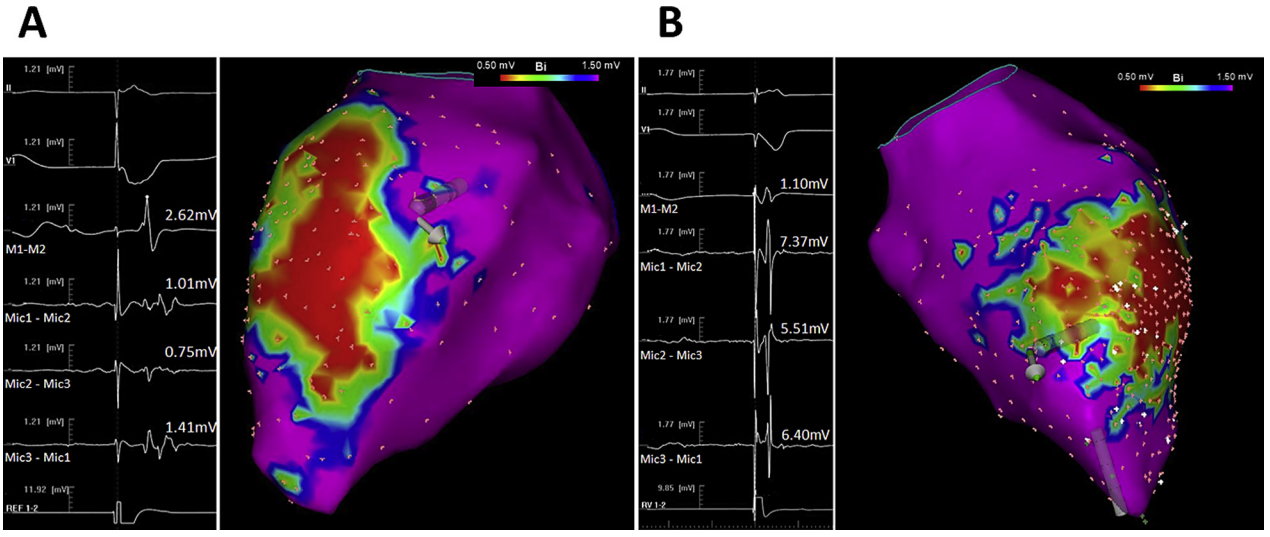

(A) Representative example of an instance in which standard electrodes underestimated the size of the scar: the standard electrodes (M1-2) recorded an electrogram with normal voltage amplitude, whereas the corresponding microelectrodes recorded fractionated low-amplitude electrograms. This suggests that the standard M1-2 electrogram was far-field, originating from the surrounding healthy tissue. **(B)** Example of an instance in which the standard electrodes overestimated the size of the scar: the standard electrodes (M1-2) recorded a low-amplitude electrogram, whereas the corresponding microelectrodes recorded high-amplitude and normal electrograms, consistent with healthy tissue. In both panels, the electroanatomic mapping was recorded with the standard electrodes.

FIGURE 6 **Endocardial LGE Surface Projection and the Comparable Electroanatomic Map**

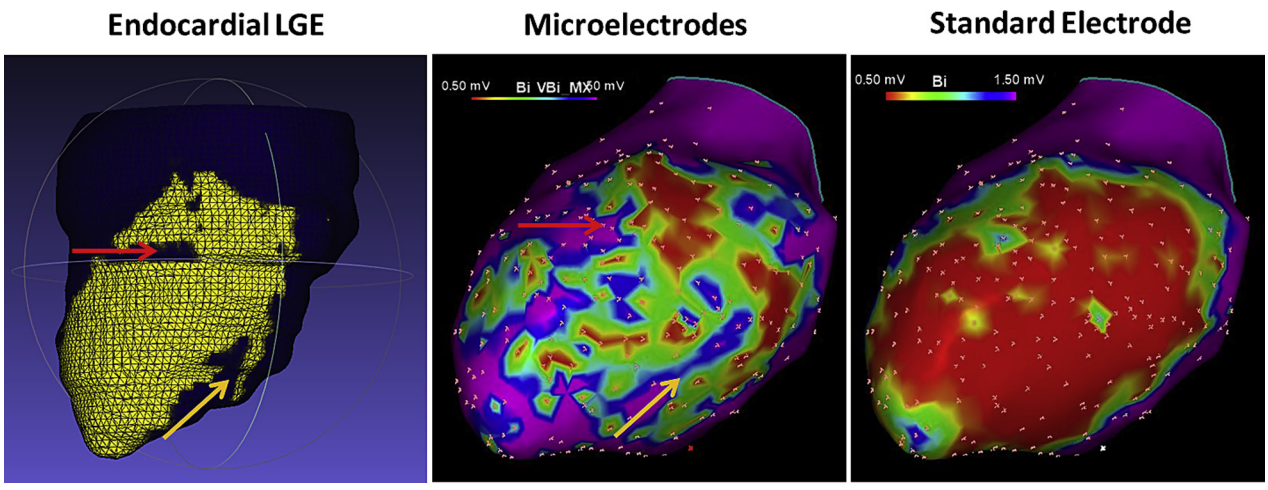

Late gadolinium enhancement (LGE) endocardial surface (0% to 33% of thickness between endocardium to epicardium) demonstrates a channel of surviving myocardial tissue at the septal border of the infarct **(left; red arrow)** and at the apical lateral border of the infarct **(left; yellow arrow)**. Electroanatomic maps at a similar projection are displayed for the microelectrodes **(middle)** and the standard electrodes **(right)**. The channels of healthy myocardium are displayed in the microelectrode map **(red and yellow arrows)** but not in the map created with standard electrodes.

corresponding EAM was not feasible, the heterogeneous distribution of collagen within the infarct and particularly in the subendocardial layer was consistent with mapping using microelectrodes (Figure 7). Overall, subendocardial myocardial fiber preservation was relatively consistent between mapping using microelectrodes, LGE, and histology (Figure 8) in the approximately identical location.

FIGURE 7 **Correlation Between Electroanatomic Mapping and Histology**

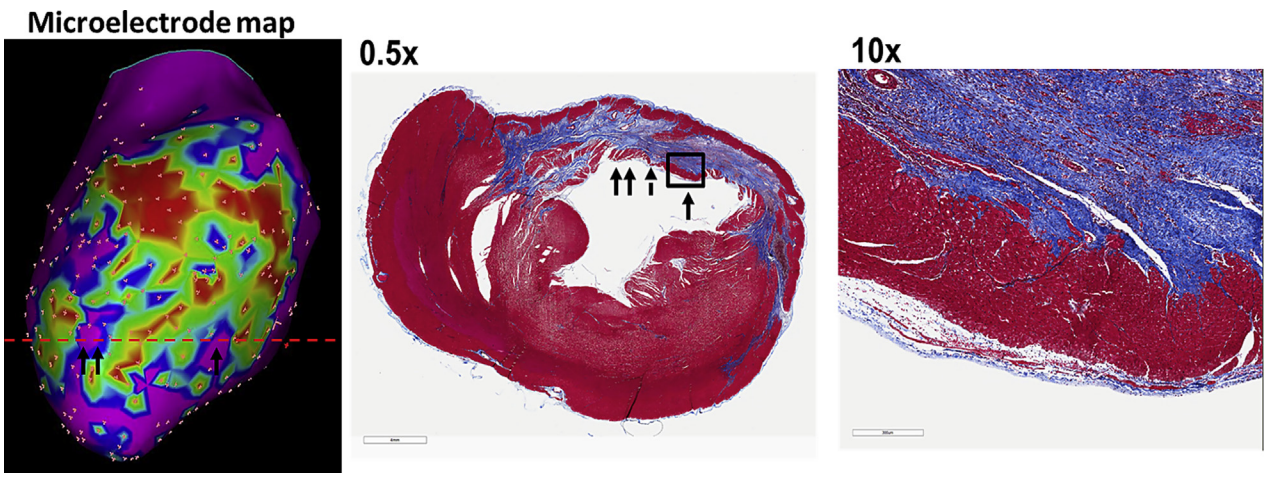

A 5-μm histological slide with Masson's trichrome staining at a level ~2.5 cm above the left ventricular apex is shown in an anterior-posterior projection **(middle)**. The histological specimen shows complex scar architecture with areas of surviving subendocardial myocardial bundles **(single and double solid arrows)** separated by subendocardial scar **(dashed arrow)**. The histological section corresponds to the dashed line of the electroanatomic map created with microelectrodes, similarly showing areas of bipolar voltage amplitude ≥1.5 mV separated by areas of low voltage (<0.5 mV). **(Right)** Higher magnification (10×) of the rectangle in the middle panel, showing surviving myocardial bundles in the subendocardium.

FIGURE 8 Multimodality Correlation Between EAM, Cardiac Magnetic Resonance, and Histology

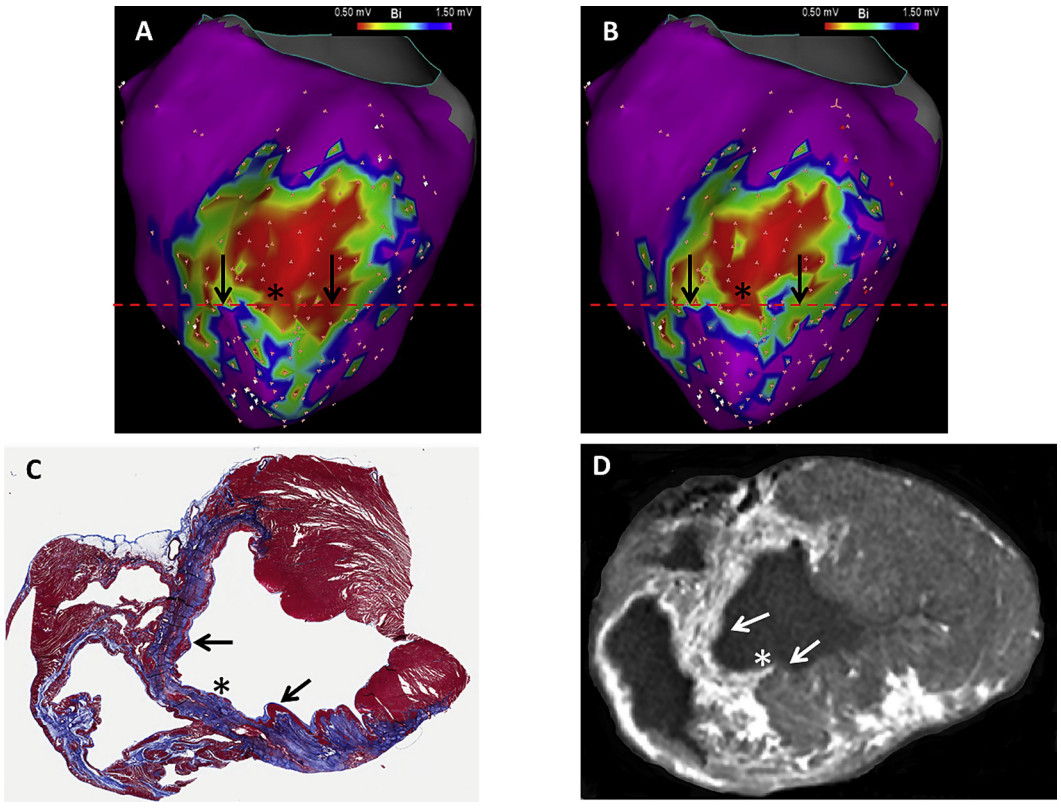

(A and B) Line of interrogation in the electroanatomic maps (EAMs) of the standard electrodes and microelectrodes, respectively. **Left arrow** is positioned at the septal border of the infarct and shows a similarly low voltage with both electrode types. **Right arrow** is positioned at the lateral border of the infarct and shows low voltage with standard electrodes and higher voltage with microelectrodes. The asterisk shows an area with very low voltage (<0.5 mV) as recorded with both types of electrodes. **(C)** Histological short-axis image with Masson's trichrome staining at the equivalent plane of interrogation showing surviving myocardial bundles **(arrows)** on both sides of an endocardial scar **(asterisk)**, consistent with the EAM created with microelectrodes. **(D)** Ex vivo cardiac magnetic resonance with late gadolinium enhancement showing an area of endocardial scar separating lateral zones of preserved subendocardium. Histological magnification is 5×.

LV PACING THRESHOLD. We compared the pacing threshold between the standard electrodes and microelectrodes in areas of low voltage (<1.5 mV) during sinus rhythm at 45 locations in 4 infarcted swine. Pacing with capture from the low-voltage zone occurred in 89% (40 of 45) with standard electrodes and in 98% (44 of 45) with microelectrodes. The pacing threshold was significantly lower with the microelectrodes (0.7 ± 1.2 mV [range 0.1 to 7.8 mV] vs. 3.6 ± 2.2 mV [range 0.2 to 8.8 mV], p = 0.001).

DISCUSSION

This study evaluated a novel catheter that combines high-resolution mapping using 3 microelectrodes with an open-irrigated, contact force ablation platform. We compared the electrogram characteristics of standard electrodes and microelectrodes in normal and infarcted LVs and examined the utility of microelectrodes for identifying channels of surviving myocardial bundles within the scar tissue compared with CMR and histology.

MAJOR FINDINGS. The major findings of this study were as follows. 1) In the healthy ventricle, the distribution of bipolar voltage amplitude is higher with microelectrodes; however, the fifth percentile is similar between electrode types and approximates the conventional cutoff value of 1.5 mV. 2) In the healthy ventricle, the unipolar electrogram amplitude measured with microelectrodes is lower than that measured with standard electrodes. 3) In the infarcted LV, microelectrodes can identify channels

of surviving myocardial bundles not identified by standard electrodes, previously presumed to be "dense scar." 4) The combination of standard and microelectrodes allows differentiation of near-field from far-field electrograms. This improves the precision for identifying borders between scar and healthy tissue (i.e., infarct border zone). 5) Pacing with capture from the low-voltage area is better achieved with microelectrodes. It is also associated with a lower pacing threshold, which potentially reduces noise and artifact related to the pacing stimulus.

UTILITY OF SMALL ELECTRODES. In the current study, we have shown that microelectrodes improve the resolution of mapping compared with standard electrodes. This adds to the growing body of literature published by our group and other groups regarding the utility of smaller electrodes with shorter interelectrode spacing for improving mapping resolution and substrate definition in both atria and ventricle (2,4,7). This difference in resolution is not solely the result of increased point density but is inherent to a smaller tissue sample, reduced averaging and cancellation effects, and data acquisition at multiple catheter orientations (4,16).

Electrograms recorded with small and closely spaced electrodes are characteristically different from electrograms recorded with standard ablation catheters. Although this has been described before, the current study strengthens previous data, because comparison between standard and small electrodes was performed at the precise same location using the same catheter. Bipolar voltage amplitude in healthy tissue was higher with microelectrodes than with standard electrodes. This observation is consistent with our previous publications comparing standard ablation catheter to a PentaRay catheter in both atria and ventricle (2,4). Several factors may explain this phenomena. 1) Smaller electrodes have a smaller "field of view, " each recording an electrical signal from spatially and temporally distinct tissue. As such, the overlap between the unipolar electrograms is smaller, resulting in lesser subtraction of one unipolar electrogram from the other and an overall larger bipolar voltage amplitude. 2) Electrogram recording with a standard linear catheter is often performed with the catheter at a perpendicular orientation relative to the chamber wall. As such, the proximal and distal signals are temporally similar, which results in significant electrogram cancellation. In contrast, the design of multielectrode mapping catheters such as the PentaRay and the studied catheter records bipolar electrograms from electrodes that are often parallel to the chamber wall and are therefore spatially and temporally distant from one another, which results in a reduced cancellation effect and an overall larger electrogram amplitude. 3) Lastly, multielectrode catheters acquire multiple simultaneous bipolar electrogram at every beat. In particular, these bipolar electrograms consist of a wide range of angles between the bipolar electrodes and the vector of propagation, from parallel (increased bipolar voltage amplitude) to perpendicular (decreased bipolar voltage amplitude). This enhances their ability to detect surviving myocardial bundles well beyond the mere difference in electrode size and spacing.

Berte et al. (7) performed LV mapping with a 3.5-mm electrode catheter (Navistar) and a multielectrode-mapping catheter (PentaRay) both in sheep with healed infarction and in patients with scar-related VT. In contrast to our findings, they reported an increased low-voltage area with multielectrode catheters. This difference might be related to inadequate tissue contact with the multielectrode mapping catheter compared with linear, tissue-contact-sensing catheters. In our study, tissue contact was inherently similar between the standard electrodes and microelectrodes. Furthermore, the authors did not corroborate the low-voltage area with either CMR or histopathology, which precludes objective assessment of the true scar.

However, catheters with small and closely spaced electrodes have a smaller field of view and record signals limited to the immediate underlying surface. Indeed, we found that unipolar voltage amplitude recorded with microelectrodes was small compared with standard electrodes. Thus, although smaller electrode catheters can enhance delineation of substrates in close proximity to the mapping surface, as in patients with post-infarction subendocardial scar, they might limit substrate outlining in patients with noncoronary disease, who often have deeper layers of disease. This novel catheter, however, combines standard-size electrodes with very small electrodes on a single platform. Such a design enhances the mapping resolution of the immediate underlying surface using the microelectrodes while allowing evaluation of the deeper layers with the standard electrodes. Importantly, the above combination of small and standard electrodes allows better differentiation of far-field from near-field electrograms to better identify borders between healthy and scar tissue and potentially between excitable and nonexcitable tissue. This could be particularly relevant for defining endpoints for substrate ablation in both atria and ventricles. The INTELLATIP MIFI catheter (Boston Scientific, Marlborough, Massachusetts) is a

clinically available ablation catheter that also incorporates small electrodes at its circumference; however, its electrodes are significantly larger (1 mm vs. ~0.15 mm), positioned 2 mm proximal to the catheter's tip, and ablation is performed via an 8-mm nonirrigated tip.

STUDY LIMITATIONS. The study was performed with an established swine model of infarction that resembles a human subendocardial infarction. Although prior research has validated bipolar voltage amplitude between swine and human, absolute values for microelectrodes require further validation in humans. Although we showed that microelectrodes were able to detect surviving myocardial bundles that were not detected by standard mapping electrodes, participation of these surviving bundles in VT was not evaluated in this study. This investigation required preservation of the tissue to allow correlation of the mapping data with ex vivo CMR and histology. We therefore refrained from ablation. In this regard, although this catheter is "2-in-1," combining high-resolution mapping with ablation, we did not evaluate its ablation capability and the effect of ablation on electrogram recordings. The correlation between EAM, CMR, and histology was made as carefully as possible; however, it is based on gross estimation. Lastly, the precise identification of a VT isthmus within the low- and very low-voltage area requires a VT study that was not performed here. A clinical VT study with ablation in humans is planned to commence shortly.

CONCLUSIONS

We evaluated a novel ablation catheter that combines high-resolution mapping using 3 microelectrodes embedded on the circumference of a standard 3.5-mm open-irrigated catheter. This catheter improves definition of scar and border zone, including identification of surviving myocardial bundles within the scar tissue. It also allows better differentiation of far-field from near-field electrograms to better characterize borders between scar and healthy tissue. It may thus serve as a single catheter to incorporate high-resolution mapping with open-irrigation tissue contact force-sensing ablation technology.

ADDRESS FOR CORRESPONDENCE: Dr. Elad Anter, Harvard-Thorndike Electrophysiology Institute, Beth Israel Deaconess Medical Center, 185 Pilgrim Road, Baker 4, Boston, Massachusetts 02215. E-mail: eanter@bidmc.harvard.edu.

PERSPECTIVES

COMPETENCY IN MEDICAL KNOWLEDGE: Mapping of ventricular scar can be enhanced by the use of catheters with smaller electrodes and closer interelectrode spacing. Use of microelectrodes embedded within a conventional ablation catheter delineates more accurately the border zone between scar and healthy tissue while limiting the need for and cost associated with the use of a separate mapping catheter.

TRANSLATIONAL OUTLOOK: High-resolution mapping with microelectrodes provides enhanced capabilities for substrate VT ablation in patients with structural heart disease. Further assessment of microelectrode utility in identifying the VT isthmus in cases of mappable and unmappable VT, as well as the clinical advantage arising from the use of microelectrodes in the acute and long-term success rates of VT ablation, is warranted.

REFERENCES

1. de Bakker JM, van Capelle FJ, Janse MJ, et al. Reentry as a cause of ventricular tachycardia in patients with chronic ischemic heart disease: electrophysiologic and anatomic correlation. Circulation 1988;77:589–606.

2. Tschabrunn CM, Roujol S, Dorman NC, Nezafat R, Josephson ME, Anter E. High-resolution mapping of ventricular scar: comparison between single and multielectrode catheters. Circ Arrhythm Electrophysiol 2016;9:e003841.

3. Tung R, Ellenbogen KA. Emergence of multielectrode mapping: on the road to higher resolution. Circ Arrhythm Electrophysiol 2016;9:e004281.

4. Anter E, Tschabrunn CM, Josephson ME. High-resolution mapping of scar-related atrial arrhythmias using smaller electrodes with closer interelectrode spacing. Circ Arrhythm Electrophysiol 2015;8:537–45.

5. Della Bella P, Bisceglia C, Tung R. Multielectrode contact mapping to assess scar modification in post-myocardial infarction ventricular tachycardia patients. Europace 2012;14 Suppl 2: ii7–12.

6. Anter E, McElderry TH, Contreras-Valdes FM, et al. Evaluation of a novel high-resolution mapping technology for ablation of recurrent scar-related atrial tachycardias. Heart Rhythm 2016;13:2048–55.

7. Berte B, Relan J, Sacher F, et al. Impact of electrode type on mapping of scar-related VT. J Cardiovasc Electrophysiol 2015;26:1213–23.

8. Tschabrunn CM, Roujol S, Nezafat R, et al. A swine model of infarct-related reentrant ventricular tachycardia: electroanatomic, magnetic resonance, and histopathological characterization. Heart Rhythm 2016;13:262–73.

9. Cassidy DM, Vassallo JA, Buxton AE, Doherty JU, Marchlinski FE, Josephson ME. The value of catheter mapping during sinus rhythm to localize site of origin of ventricular tachycardia. Circulation 1984;69:1103–10.

10. Cassidy DM, Vassallo JA, Marchlinski FE, Buxton AE, Untereker WJ, Josephson ME. Endocardial mapping in humans in sinus rhythm with normal left ventricles: activation patterns and characteristics of electrograms. Circulation 1984;70:37–42.

11. Moghari MH, Chan RH, Hong SN, et al. Free-breathing cardiac MR with a fixed navigator efficiency using adaptive gating window size. Magn Reson Med 2012;68:1866–75.

12. Akcakaya M, Basha TA, Goddu B, et al. Low-dimensional-structure self-learning and thresholding: regularization beyond compressed sensing for MRI reconstruction. Magn Reson Med 2011;66:756–67.

13. Akcakaya M, Rayatzadeh H, Basha TA, et al. Accelerated late gadolinium enhancement cardiac MR imaging with isotropic spatial resolution using compressed sensing: initial experience. Radiology 2012;264:691–9.

14. Flett AS, Hasleton J, Cook C, et al. Evaluation of techniques for the quantification of myocardial scar of differing etiology using cardiac magnetic resonance. JCMG: J Am Coll Cardiol Img 2011;4:150–6.

15. Cignoni P, Callieri M, Corsini M, Dellepiane M, Ganovelli F, Ranzuglia G. MeshLab: an open-source mesh processing tool. Computing 2008;1:129–36.

16. Anter E, Josephson ME. Bipolar voltage amplitude: what does it really mean? Heart Rhythm 2016;13:326–7.

KEY WORDS electrodes, mapping, microelectrodes, post-infarct, ventricular tachycardia

APPENDIX For supplemental figures, please see the online version of this article.